JACS
JOURNAL OF THE AMERICAN CHEMICAL SOCIETY
Communication
pubs.acs.org/JACS

Subtle Ligand Modification Inverts Guest Binding Hierarchy in $M^{II}_8L_6$ Supramolecular Cubes

William J. Ramsay,[†] Felix J. Rizzuto,[†] Tanya K. Ronson, Kenji Caprice, and Jonathan R. Nitschke*

Department of Chemistry, University of Cambridge, Cambridge, United Kingdom CB2 1EW

Supporting Information

ABSTRACT: Zinc(II), a dimolybdenum(II) paddlewheel tetramine **A**, and 2-formylpyridine self-assembled to generate a cubic $Zn^{II}_8(\mathbf{L^A})_6$ assembly. The paddlewheel faces of this assembly exhibited two distinct conformations, whereas the analogous $Fe^{II}_8(\mathbf{L^A})_6$ framework displayed no such perturbation to its structure. This variation in behavior is attributed to the subtle difference in ligand rotational freedom between the Zn^{II}- and Fe^{II}-cornered cubes. The incorporation of a fluorinated Mo^{II}_2 paddlewheel, **B**, into analogous $Zn^{II}_8(\mathbf{L^B})_6$ and $Fe^{II}_8(\mathbf{L^B})_6$ structures resulted in changes to the rotational dynamics of the ligands. These differing dynamics perturbed the energies of the frontier orbitals of these structures, as determined through spectroscopic and electrochemical methods. The result of these perturbations was an inversion of the halide binding preference of the $Zn^{II}_8(\mathbf{L^B})_6$ host as compared to its $Zn^{II}_8(\mathbf{L^A})_6$ congener, whereas the $Fe^{II}_8(\mathbf{L^B})_6$ host maintained a similar binding hierarchy to $Fe^{II}_8(\mathbf{L^A})_6$.

Metal−organic self-assembly has produced a diverse array of functional three-dimensional structures recently,[1] as rationality has eclipsed serendipity to enable designs of increasing intricacy.[2] Many of these structures contain void spaces[3] within which one or more guests may bind,[4] allowing the form and reactivities of these guests to be modulated in well-defined ways.[5]

In others' work[6] and in our own, the use of subcomponent self-assembly, involving the simultaneous use of dynamic C═N and N→Metal linkages for construction,[7] has permitted the generation of many different architectures from near-identical subcomponents.[8] Product identities can change dramatically as a result of slight disturbances in the forces holding these structures together; a change in solvent[9] or anion,[10] or subcomponent substitution,[11] can lead to very different structural outcomes. Lessons learned as a result can be implemented to design new architectures with tailored functions.

In other cases, however, structural outcomes are not perturbed by changes in the factors noted above: Planar tetramine subcomponents, for example, are observed exclusively to form cubic capsules with a M_8L_6 stoichiometry, rejecting added components even if the M:L ratio is perturbed by ∼20%.[12] Given the certainty of this structural outcome of the self-assembly reaction, we sought to explore whether perturbations to the host−guest chemistry of a cubic $Fe^{II}_8L_6$ product[12b] could be engineered through slight chemical modifications of the subcomponents or by changing the identity of the metal template. To this end, the host−guest chemistry of cubes **1**−**4** (Scheme 1) was explored. These cubes were prepared using

Scheme 1. Assembly of Cubic Structures 1−4

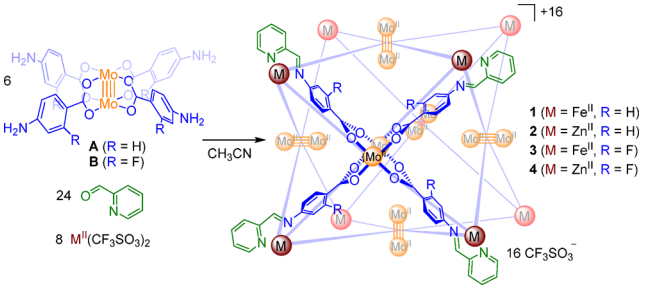

either Zn^{II} or Fe^{II} to define the vertices, and with either nonfluorinated tetramine **A** or quadruply fluorinated tetramine **B** to form the faces. While **1**−**4** are outwardly of the same shape and size, subtle differences were observed between them, such as phenyl ring rotation behavior and M−O bond flexibility. These differences manifested as an inversion of the halide binding preference between **2** and **4**. This result highlights the substantial influences of small electronic and steric perturbations upon the behaviors of hollow cages in solution, providing insight into the factors affecting host−guest interactions at the nanoscale.

The syntheses of **1**[12b]−**4** are shown in Scheme 1 and described in Supporting Information (SI) Section 1. Although the ^{1}H NMR spectrum of the Fe^{II}-cornered structure **1** displayed distinct signals for each of the protons of the ligand, implying slow rotation of the phenylene rings on the NMR time scale (Figure S1),[12b] the ^{1}H NMR spectrum of **2** at room temperature was unexpectedly complex. Overlaid upon a symmetrical set of ligand resonances (consistent with phenylene rotation), multiple, lower intensity signals were observed (Figure S2); however, DOSY NMR gave results consistent with the formation of a single species (Figure S5). Electrospray (ESI) MS gave results consistent with the formation of the anticipated cubic structure (Figures S6 and S7).

Single-crystal X-ray diffraction (SI Section 2.1) revealed the solid-state structure of **2** (Figure 1). The faces of cube **2** consist of six dimolybdenum(II) paddlewheels, with a Zn−Zn distance of 19.0 Å diagonally across the faces. As this distance in **1** measured 18.7 Å, **2** encloses nearly the same cavity volume (565 Å^3, Figure S11) as **1**[12b] (559 Å^3). Although triflate coordination to the

Received: April 14, 2016
Published: May 23, 2016

DOI: 10.1021/jacs.6b03858
J. Am. Chem. Soc. 2016, 138, 7264−7267

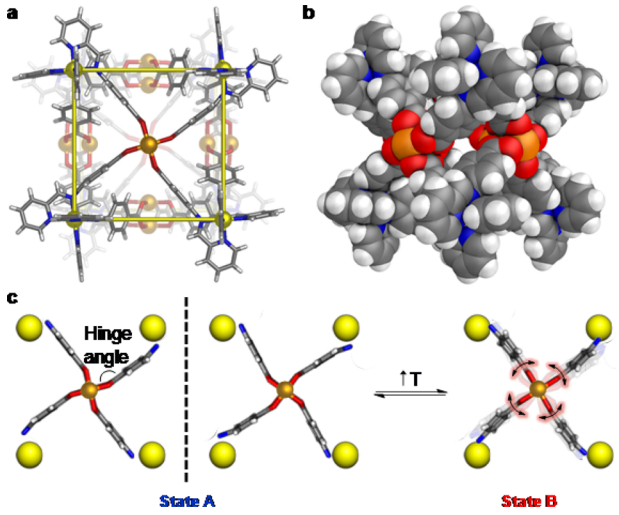

Figure 1. (a) X-ray crystal structure of **2**, viewed perpendicular to a face (yellow lines highlight the edges of the cubic framework); (b) space-filling representation of **2** viewed down the cube edge (axially coordinating species, noncoordinated anions, and solvent molecules omitted for clarity). (c) Left: Schematic representations of the two diastereomerically distinct configurations of how a ligand may span the four Zn^{II} corners (yellow spheres) of a single cube face of **2** (a right or left twist of the face, State A), observed predominantly in solution below 273 K. Right: When heated above 300 K, an averaging of the configurations is inferred to result in simplified NMR spectra (State B). Color scheme: C, gray; O, red; N, blue; Zn, yellow; H, white; Mo, orange.

molybdenum centers was observed in both the solution and solid-state structure of **1**,[12b] no evidence of triflate coordination with **2** was observed in solution by ^{19}F NMR (Figure S8) or in the solid state.

The X-ray structure revealed a "hinge angle" of 159° (Figure 1c) between the carboxylate groups and the Mo^{II}_2 moieties of **2**, instead of the 180° coordination observed in the case of **1**. Although only one diastereoisomer was observed in the crystal, models suggest that both left- and right-handed propeller configurations of the ligand (Figure 1c, State A) could coexist within a single framework of **2** with minimal energetic penalty. We infer the complexity of the ^1H NMR spectrum of **2** to be due to the presence of a mixture of both ligand configurations across the faces of the cube. The predominance of one configuration—possibly the one observed in the crystal—thus accounts for the set of symmetrical ^1H NMR peaks, and the other configurations give rise to the lower-intensity signals (Figure S2).

Upon heating, the ^1H NMR spectrum of **2** is observed to simplify (Figure S9). We infer this process to involve the coalescence of signals from the many diastereomers of **2** (Figure 1c, State A) into a regime where "hinge flipping" is occurring rapidly on the NMR time scale (Figure 1c, State B). The energy difference between states (ΔG°) was determined to be 31 kJ mol^{-1} (Figure S10). The dynamic behavior of the ligands in **2** thus emerges from its $Zn^{II}_8L_6$ framework in a way not observed in the $Fe^{II}_8L_6$ congeners **1**[12b] and **3** (see below), possibly because the more flexible coordination sphere of Zn^{II} allows different configurations of **2** to be adopted.

As a fluoro substituent represented only a minor steric perturbation to the structure of **A**, paddlewheel subcomponent **B**, bearing *ortho*-fluorine atoms on its *p*-aminobenzoate substituents (Scheme 1), was prepared in order to probe the subtle steric effects and more substantial electronic effects of its fluoro substituents upon the dynamics of cage frameworks into which it was incorporated, and ultimately upon guest binding.

Although the reaction between **B** (6 equiv), 2-formylpyridine (24 equiv), and iron(II) triflate (8 equiv) in acetonitrile produced a deep-red solution consistent with the formation of **3** (SI Section 1.5), the signals in the ^1H NMR spectrum were broad (Figure S13). DOSY NMR indicated that a structure with a similar hydrodynamic radius to that of **1** had assembled in solution (Figure S16), and ESI-MS (Figures S17 and S18) gave results consistent with a $Fe^{II}_8L_6$ formulation.

Single crystal X-ray diffraction revealed the cubic structure of **3** (Figure 2). Slightly larger than **1**, cube **3** has Fe−Fe distances

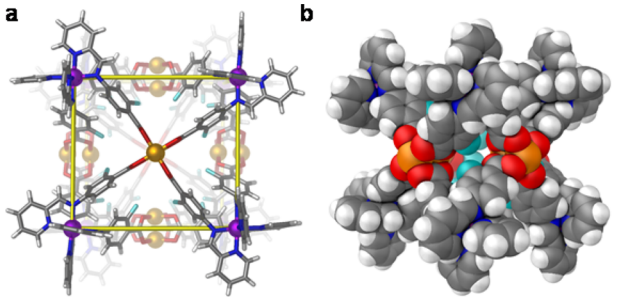

Figure 2. (a) Wire-frame representation of the X-ray crystal structure of **3** (the edges of the cubic framework are highlighted by yellow lines) and (b) space-filling representation (axially coordinating species, non-coordinated anions, and solvent molecules removed for clarity). Color scheme: Fe, purple; F, teal. Only the major occupancy positions of disordered groups are shown for clarity.

averaging 19.2 Å diagonally across the face. The Mo−Mo bond lengths in **3** (2.109(1)−2.113(1) Å) are also slightly longer than those in **1** (2.063(1)−2.076(1) Å). The fluorine atoms are disordered between *endo* and *exo* configurations throughout, with ~70% pointing inward and 30% outward. The cavity volume of **3** is 546 $Å^3$ (SI Section 1.5.1) for a configuration in which all fluoro substituents point inward.

The ^1H and ^{19}F NMR spectra of **3** (Figures S13 and S19) are consistent with rapid rotation of the fluorophenylene rings, even at 233 K (Figures S20 and S21), whereas for **1** the phenylene rings appear not to be rotating.[12b] We hypothesize that the fluoro substituents encounter electronic and steric repulsion[13] when eclipsing the carboxylate oxygens, thus raising the energy of the configuration where fluorophenylene and carboxylate are coplanar, in **B** and **3**, relative to the energy of this ground state in the case of **1**. Whereas the energies of the transition states during rotation are similar in **1** and **3**, where the phenylene or fluorophenylene lies orthogonal to the carboxylate plane, this ground-state destabilization effect is inferred to lead to the rapid rotation observed in **3**, contrasting with the slow rotation observed for **1**.

Analogously to **3**, cube **4** self-assembled from **B**, 2-formylpyridine and zinc(II) triflate (SI Section 1.6). The ligand signals in the ^1H NMR spectrum were sharp and symmetric (Figure S23), indicating that diastereomers of the type observed for **2** were not present or were interconverting rapidly on the NMR time scale; no asymmetry could be observed even upon cooling to 233 K (Figures S27 and S28). A similar DOSY diffusion coefficient to that of **2** was observed (Figure S29), and the composition of **4** was confirmed by mass spectrometry (Figures S30 and S31). As with **2** (Figure S19),

DOI: 10.1021/jacs.6b03858
J. Am. Chem. Soc. 2016, 138, 7264−7267

there was no interaction of triflate with host **4** observable by ^{19}F NMR spectroscopy (Figure S32).

As **1** had been observed to bind a single halide anion to its interior molybdenum coordination sites,[12b] we investigated halide binding in **2**–**4**. Given the differences exhibited by the ligands in these hosts in solution, significant differences in guest interactions were anticipated, due to the subtle structural, dynamic, electronic, and steric differences as they related to host–guest binding across the set of close congeners **1**–**4**.

UV–vis spectroscopy enabled the quantification of the strengths of interactions of various halides with cubes **2**–**4** (Figures S34, S39, and S48). Progressive addition of fluoride, chloride, bromide, or iodide in all cases resulted in a decrease in the intensity of the metal-to-ligand charge-transfer (MLCT) absorption associated with the tetracarboxylato(dimolybdenum) chromophore of the host,[14] along with the appearance of stable isosbestic points. The 1:1 halide binding affinities of hosts **1**–**4** are summarized in Table 1: While hosts **1**–**3** bound iodide more strongly than fluoride, host **4** was observed to bind fluoride with the highest affinity.

Table 1. Binding Constants (K_a, × 10^4 M^{-1}) of Halides (as Tetrabutylammonium Salts) with Cubic Hosts 1–4 (Determined at 298 K in Acetonitrile)

guest	**1**[12b]	**2**	**3**	**4**
F^-	0.49 ± 0.06	0.8 ± 0.3	2.4 ± 0.5	8.1 ± 0.5
Cl^-	0.5 ± 0.1	1.0 ± 0.2	6.1 ± 0.7	5.2 ± 0.8
Br^-	1.7 ± 0.4	1.3 ± 0.3	9.1 ± 0.7	3.3 ± 0.3
I^-	3.8 ± 0.4	1.7 ± 0.5	22 ± 2	2.3 ± 0.7

Furthermore, fluorination of a paddlewheel in both cases increased the halide affinity of its corresponding $M^{II}_8L_6$ cube. We initially ascribed this improvement to the slight contraction of the void space of **3** and **4**, as compared to **1** and **2**; however, this change does not account for the inversion of the binding hierarchy observed in **4**. Comparison of the UV–vis spectra of subcomponents **A** and **B** helped clarify the reasons behind this change in binding strength: The $Mo_2(O_2CR)_4$ $\delta \rightarrow \pi^*$ MLCT transition in paddlewheel **A** (426 nm) was observed to increase in energy in **B** (400 nm), providing an initial indication that fluorinating the paddlewheel would widen the HOMO/LUMO gaps of the architectures into which they assembled.

We infer that the presence or absence of fluoro substituents and the choice of Fe^{II} vs Zn^{II} together influence the preference of the molybdenum centers for hard or soft bases. To quantify these effects, the energies of the Mo_2 δ (HOMO) orbitals were determined for hosts **1**–**4** using cyclic voltammetry (CV),[15] and their HOMO/LUMO gaps (ΔE) were determined by UV–vis spectroscopy, enabling the back-calculation of CO_2 π^* LUMO energies (SI Section 4). Our results are provided in Figure 3.

The similar halide binding hierarchy and affinities of **1** and **2** are reflected in their similar orbital energies and HOMO/LUMO gaps; however, substantially different responses to guests are observed upon fluorination, despite the consistent lowering of both HOMO and LUMO energies in **3** and **4**. In the case of Zn^{II}-cornered architecture **2**, fluorination results in a widening of the HOMO/LUMO gap in **4**, consistent with the trend observed for the free subcomponents, whereas for the Fe^{II}-cornered structures, the HOMO/LUMO gap is observed to contract in going from **1** to fluorinated **3**.

We hypothesize that in **1**, restricted rotation of the phenyl groups brings the electron-withdrawing Fe^{II} center into effective

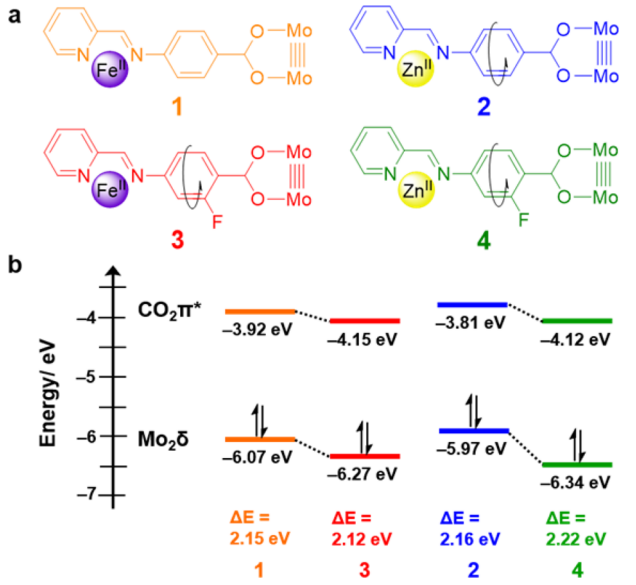

Figure 3. (a) The asymmetric units of structures **1**–**4**, showing schematically the free rotation on the NMR time scale observed for **2**–**4**. (b) Energy diagram displaying the measured $Mo_2\delta$ HOMO and $CO_2\pi^*$ LUMO energies of **1**–**4** from CV and UV–vis data.

conjugation with the Mo^{II} binding sites and that this conjugation is weakened in **3** due to the free rotation of the phenylene groups. We thus propose that the inductive effect of ligand fluorination upon the HOMO energy of **1** is counterbalanced by this loss of conjugation, lessening the impact of ligand fluorination in **3**.

For the Fe^{II}-cornered cubes, fluorination resulted in an order of magnitude increase in the binding affinity for each halide to **3** relative to **1**; however, for the Zn^{II}-cornered cubes, the binding affinity for hard bases was observed to improve more dramatically than for soft bases upon fluorination (an order of magnitude increase vs a doubling, respectively, in **4** relative to **2**) (Table 1). We attribute this trend to a greater hardening of the molybdenum centers in **4**, as compared to **3**, as reflected in the greater lowering of the HOMO energy and the increased HOMO/LUMO gap of **4**. Fluorination thus results in **4** exhibiting the highest affinity for hard bases, whereas **3** (which also binds hard bases more strongly than either **1** or **2**) binds softer halides more strongly than any other cube. A combination of subtle ligand dynamics and inductive effects thus serves to shape guest binding.

The interaction of halides with **3** was also monitored by ^{19}F NMR spectroscopy in addition to the UV–vis titrations (SI Section 3.2). The broad ^{19}F NMR signal for triflate observed in the case of **1**[12b] was observed as a sharp peak in the case of **3**. This signal moved to the chemical shift value associated with free triflate upon addition of halide, consistent with triflate displacement by the more strongly coordinating anions. Titrations carried out using ^{1}H NMR spectroscopy indicated minimal changes across the series of hosts **1**–**4** (the ^{19}F signals for hosts **2** and **4** also did not change significantly), suggesting that halide exchange was rapid on the NMR time scale and did not significantly perturb the environment of the ligand protons (SI Section 3).

This study demonstrates how the choice of corner metal centers in the construction of heterometallic supramolecular cubes **1** and **2** can influence the rotational freedom of the ligands in solution, providing a means to tailor the dynamic behavior of the host. Ligand fluorination in hosts **3** and **4** further modified

DOI: 10.1021/jacs.6b03858
J. Am. Chem. Soc. 2016, 138, 7264–7267

the guest binding properties by altering both the dynamic behavior of the ligand and the electronics of the molybdenum coordination sites. We envisage that further systematic tailoring of the steric and electronic properties of substituents on the frameworks of metal−organic assemblies will engender new modes of controlling their interactions with other species within chemical systems, enabling the tailored design of function for specific needs and purposes.[16]

■ ASSOCIATED CONTENT

Supporting Information

The Supporting Information is available free of charge on the ACS Publications website at DOI: 10.1021/jacs.6b03858.

Characterization data for **2**−**4**, anion binding studies, CV and UV−vis data (PDF)

X-ray crystallography data for **2** (CCDC 1432685) (CIF)

X-ray crystallography data for **3** (CCDC 1432686) (CIF)

■ AUTHOR INFORMATION

Corresponding Author

*jrn34@cam.ac.uk

Author Contributions

†These authors contributed equally.

Notes

The authors declare no competing financial interest.

■ ACKNOWLEDGMENTS

This work was supported by the EU FP7 Marie Curie Academic-Industrial Initial Training Network on Dynamic Molecular Nanostructures (DYNAMOL) and the UK Engineering and Physical Sciences Research Council (EPSRC EP/M008258/1). F.J.R. acknowledges Cambridge Australia Scholarships for Ph.D. funding. We thank Diamond Light Source (U.K.) for synchrotron beamtime on I19 (MT8464) and the NMR facility at the Department of Chemistry.

■ REFERENCES

(1) (a) Han, M.; Michel, R.; He, B.; Chen, Y.-S.; Stalke, D.; John, M.; Clever, G. H. *Angew. Chem., Int. Ed.* **2013**, *52*, 1319. (b) Fujita, D.; Suzuki, K.; Sato, S.; Yagi-Utsumi, M.; Yamaguchi, Y.; Mizuno, N.; Kumasaka, T.; Takata, M.; Noda, M.; Uchiyama, S.; Kato, K.; Fujita, M. *Nat. Commun.* **2012**, *3*, 1093. (c) Nakamura, T.; Ube, H.; Shionoya, M. *Angew. Chem., Int. Ed.* **2013**, *52*, 12096. (d) Chifotides, H. T.; Giles, I. D.; Dunbar, K. R. *J. Am. Chem. Soc.* **2013**, *135*, 3039. (e) Frischmann, P. D.; MacLachlan, M. J. *Chem. Soc. Rev.* **2013**, *42*, 871. (f) Li, F.; Clegg, J. K.; Goux-Capes, L.; Chastanet, G.; D'Alessandro, D. M.; Létard, J.-F.; Kepert, C. J. *Angew. Chem., Int. Ed.* **2011**, *50*, 2820. (g) Su, X.; Aprahamian, I. *Chem. Soc. Rev.* **2014**, *43*, 1963.

(2) (a) Saalfrank, R. W.; Maid, H.; Scheurer, A. *Angew. Chem., Int. Ed.* **2008**, *47*, 8794. (b) Custelcean, R.; Bosano, J.; Bonnesen, P. V.; Kertesz, V.; Hay, B. P. *Angew. Chem., Int. Ed.* **2009**, *48*, 4025. (c) Pitt, M. A.; Johnson, D. W. *Chem. Soc. Rev.* **2007**, *36*, 1441. (d) Aliprandi, A.; Mauro, M.; De Cola, L. *Nat. Chem.* **2016**, *8*, 10.

(3) Cook, T. R.; Stang, P. J. *Chem. Rev.* **2015**, *115*, 7001.

(4) (a) Samanta, S. K.; Schmittel, M. *Org. Biomol. Chem.* **2013**, *11*, 3108. (b) Schneider, H.-J.; Yatsimirsky, A. K. *Chem. Soc. Rev.* **2008**, *37*, 263. (c) Kishi, N.; Akita, M.; Yoshizawa, M. *Angew. Chem., Int. Ed.* **2014**, *53*, 3604. (d) Fiedler, D.; Leung, D. H.; Bergman, R. G.; Raymond, K. N. *Acc. Chem. Res.* **2005**, *38*, 349. (e) Garai, S.; Rubčić, M.; Bögge, H.; Haupt, E. T. K.; Gouzerh, P.; Müller, A. *Angew. Chem., Int. Ed.* **2015**, *54*, 5879. (f) Evans, N. H.; Beer, P. D. *Angew. Chem., Int. Ed.* **2014**, *53*, 11716. (g) Wang, Q.-Q.; Day, V. W.; Bowman-James, K. *Angew. Chem., Int. Ed.* **2012**, *51*, 2119. (h) Hooley, R. J.; Shenoy, S. R.; Rebek, J. *Org. Lett.* **2008**, *10*, 5397. (i) Smith, M. K.; Miljanic, O. S. *Org. Biomol. Chem.* **2015**, *13*, 7841.

(5) (a) Zhang, Q.; Tiefenbacher, K. *Nat. Chem.* **2015**, *7*, 197. (b) Hastings, C. J.; Pluth, M. D.; Bergman, R. G.; Raymond, K. N. *J. Am. Chem. Soc.* **2010**, *132*, 6938. (c) Jing, X.; He, C.; Yang, Y.; Duan, C. *J. Am. Chem. Soc.* **2015**, *137*, 3967. (d) Nishioka, Y.; Yamaguchi, T.; Kawano, M.; Fujita, M. *J. Am. Chem. Soc.* **2008**, *130*, 8160. (e) Liu, S.; Gan, H.; Hermann, A. T.; Rick, S. W.; Gibb, B. C. *Nat. Chem.* **2010**, *2*, 847.

(6) (a) Luo, D.; Zhou, X.-P.; Li, D. *Inorg. Chem.* **2015**, *54*, 10822. (b) Ayme, J.-F.; Beves, J. E.; Leigh, D. A.; McBurney, R. T.; Rissanen, K.; Schultz, D. *J. Am. Chem. Soc.* **2012**, *134*, 9488. (c) Feltham, H. L. C.; Klower, F.; Cameron, S. A.; Larsen, D. S.; Lan, Y.; Tropiano, M.; Faulkner, S.; Powell, A. K.; Brooker, S. *Dalton Trans.* **2011**, *40*, 11425. (d) Pascu, G. I.; Hotze, A. C. G.; Sanchez-Cano, C.; Kariuki, B. M.; Hannon, M. J. *Angew. Chem., Int. Ed.* **2007**, *46*, 4374. (e) Mastalerz, M.; Oppel, I. M. *Eur. J. Org. Chem.* **2011**, *2011*, 5971. (f) Frischmann, P. D.; Kunz, V.; Stepanenko, V.; Würthner, F. *Chem. - Eur. J.* **2015**, *21*, 2766. (g) Bunzen, H.; Nonappa; Kalenius, E.; Hietala, S.; Kolehmainen, E. *Chem. - Eur. J.* **2013**, *19*, 12978. (h) Lewing, D.; Koppetz, H.; Hahn, F. E. *Inorg. Chem.* **2015**, *54*, 7653.

(7) Nitschke, J. R. *Acc. Chem. Res.* **2007**, *40*, 103.

(8) Ronson, T. K.; Zarra, S.; Black, S. P.; Nitschke, J. R. *Chem. Commun.* **2013**, *49*, 2476.

(9) (a) Bilbeisi, R. A.; Ronson, T. K.; Nitschke, J. R. *Angew. Chem., Int. Ed.* **2013**, *52*, 9027. (b) Zarra, S.; Clegg, J. K.; Nitschke, J. R. *Angew. Chem., Int. Ed.* **2013**, *52*, 4837.

(10) (a) Riddell, I. A.; Smulders, M. M. J.; Clegg, J. K.; Hristova, Y. R.; Breiner, B.; Thoburn, J. D.; Nitschke, J. R. *Nat. Chem.* **2012**, *4*, 751. (b) Ayme, J.-F.; Beves, J. E.; Leigh, D. A.; McBurney, R. T.; Rissanen, K.; Schultz, D. *Nat. Chem.* **2012**, *4*, 15.

(11) Wood, C. S.; Ronson, T. K.; Belenguer, A. M.; Holstein, J. J.; Nitschke, J. R. *Nat. Chem.* **2015**, *7*, 354.

(12) (a) Meng, W.; Breiner, B.; Rissanen, K.; Thoburn, J. D.; Clegg, J. K.; Nitschke, J. R. *Angew. Chem., Int. Ed.* **2011**, *50*, 3479. (b) Ramsay, W. J.; Ronson, T. K.; Clegg, J. K.; Nitschke, J. R. *Angew. Chem., Int. Ed.* **2013**, *52*, 13439. (c) Otte, M.; Kuijpers, P. F.; Troeppner, O.; Ivanović-Burmazović, I.; Reek, J. N. H.; de Bruin, B. *Chem. - Eur. J.* **2013**, *19*, 10170.

(13) Lunazzi, L.; Mancinelli, M.; Mazzanti, A.; Lepri, S.; Ruzziconi, R.; Schlosser, M. *Org. Biomol. Chem.* **2012**, *10*, 1847.

(14) (a) Chisholm, M. H.; Gustafson, T. L.; Turro, C. *Acc. Chem. Res.* **2012**, *46*, 529. (b) Cotton, F. A.; Norman, J. G. *J. Coord. Chem.* **1972**, *1*, 161.

(15) Cardona, C. M.; Li, W.; Kaifer, A. E.; Stockdale, D.; Bazan, G. C. *Adv. Mater.* **2011**, *23*, 2367.

(16) (a) Gianneschi, N. C.; Masar, M. S.; Mirkin, C. A. *Acc. Chem. Res.* **2005**, *38*, 825. (b) Busschaert, N.; Caltagirone, C.; Van Rossom, W.; Gale, P. A. *Chem. Rev.* **2015**, *115*, 8038. (c) Ma, X.; Zhao, Y. *Chem. Rev.* **2015**, *115*, 7794. (d) Brachvogel, R.-C.; Hampel, F.; von Delius, M. *Nat. Commun.* **2015**, *6*, 7129.

DOI: 10.1021/jacs.6b03858
J. Am. Chem. Soc. 2016, 138, 7264−7267